CrossMark

A tunable delivery platform to provide local chemotherapy for pancreatic ductal adenocarcinoma

Laura Indolfi [a, b, *, 1], Matteo Ligorio [b, c, 1], David T. Ting [b, **, 1], Kristina Xega [b], Abraham R. Tzafriri [d], Francesca Bersani [b], Nicola Aceto [b], Vishal Thapar [b], Bryan C. Fuchs [b], Vikram Deshpande [b], Aaron B. Baker [e], Cristina R. Ferrone [b], Daniel A. Haber [b, f], Robert Langer [a, g, 1], Jeffrey W. Clark [b, 1], Elazer R. Edelman [a, h, 1]

[a] Institute for Medical Engineering and Science, Massachusetts Institute of Technology, Cambridge, MA, USA
[b] Departments of Surgery, Medicine, and Pathology, Massachusetts General Hospital, Harvard Medical School, Boston, MA, USA
[c] Department of Health Sciences, University of Genoa, Genoa, Italy
[d] CBSET Inc., Department of Applied Sciences, Lexington, MA, USA
[e] Department of Biomedical Engineering, University of Texas at Austin, Austin, TX, USA
[f] Howard Hughes Medical Institute, Chevy Chase, MD, USA
[g] The David H. Koch Institute for Integrative Cancer Research, Massachusetts Institute of Technology, Cambridge, MA, USA
[h] Cardiovascular Division, Department of Medicine, Brigham and Women's Hospital, Harvard Medical School, Boston, MA, USA

ARTICLE INFO

ABSTRACT

Pancreatic ductal adenocarcinoma (PDAC) is one of the most devastating and painful cancers. It is often highly resistant to therapy owing to inherent chemoresistance and the desmoplastic response that creates a barrier of fibrous tissue preventing transport of chemotherapeutics into the tumor. The growth of the tumor in pancreatic cancer often leads to invasion of other organs and partial or complete biliary obstruction, inducing intense pain for patients and necessitating tumor resection or repeated stenting. Here, we have developed a delivery device to provide enhanced palliative therapy for pancreatic cancer patients by providing high concentrations of chemotherapeutic compounds locally at the tumor site. This treatment could reduce the need for repeated procedures in advanced PDAC patients to debulk the tumor mass or stent the obstructed bile duct. To facilitate clinical translation, we created the device out of currently approved materials and drugs. We engineered an implantable poly(lactic-co-glycolic)-based biodegradable device that is able to linearly release high doses of chemotherapeutic drugs for up to 60 days. We created five patient-derived PDAC cell lines and tested their sensitivity to approved chemotherapeutic compounds. These in vitro experiments showed that paclitaxel was the most effective single agent across all cell lines. We compared the efficacy of systemic and local paclitaxel therapy on the patient-derived cell lines in an orthotopic xenograft model in mice (PDX). In this model, we found up to a 12-fold increase in suppression of tumor growth by local therapy in comparison to systemic administration and reduce retention into off-target organs. Herein, we highlight the efficacy of a local therapeutic approach to overcome PDAC chemoresistance and reduce the need for repeated interventions and biliary obstruction by preventing local tumor growth. Our results underscore the urgent need for an implantable drug-eluting platform to deliver cytotoxic agents directly within the tumor mass as a novel therapeutic strategy for patients with pancreatic cancer.

© 2016 Elsevier Ltd. All rights reserved.

* Corresponding author. Institute of Medical Engineering and Science, Massachusetts Institute of Technology, 77 Massachusetts Avenue, Building E25-449, Cambridge, MA 02139, USA.
** Corresponding author. Massachusetts General Hospital Cancer Center, Harvard Medical School, 149 13th St., CNY149 6-618B, Charlestown, MA 02129, USA.
E-mail addresses: lindolfi@mit.edu (L. Indolfi), dting1@mgh.harvard.edu (D.T. Ting).
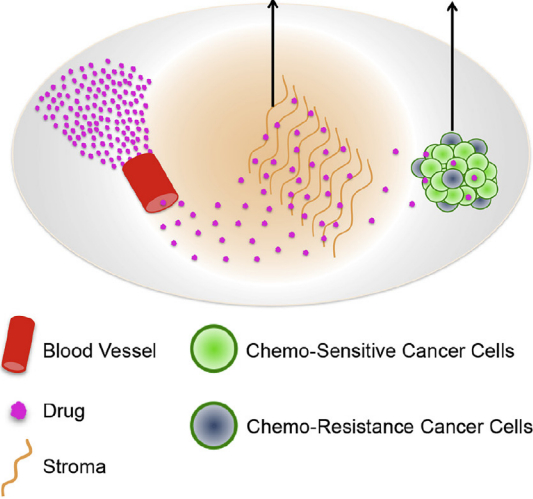[1] These authors contributed equally to this work.

1. Introduction

Pancreatic cancer is one of the most lethal adult cancers, having a 5-year overall survival rate less than 6%. At the time of diagnosis, only 20% of patients have localized disease that can be successfully treated by surgical resection. The vast majority of PDAC patients
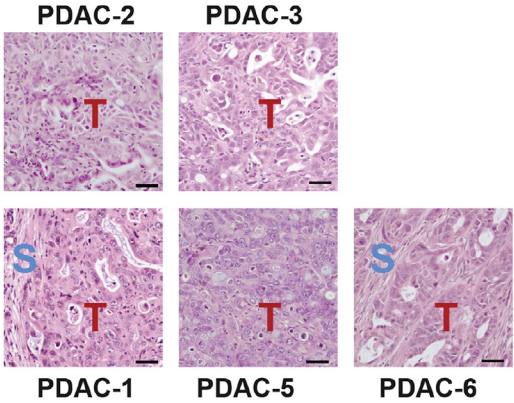
have locally advanced disease, which limits the therapeutic options to radiation and systemic chemotherapies. By invading the surrounding vital organs, locally advanced tumors cause excruciating symptoms in patients including intense abdominal pain, anorexia, nausea, vomiting and jaundice. A major source of suffering for pancreatic cancer patients is the development of biliary obstruction due to the growth of the tumor into the biliary duct. This obstruction often requires repeated procedures to clear the duct through resection or stenting.

An additional issue with treatment of pancreatic cancer is the development of chemotherapeutic resistance. Pancreatic cancer is often highly resistant to chemotherapy due to intrinsic cellular chemoresistance, hypovascularity [1–4] and an extensive desmoplastic reaction that creates a barrier of fibrous tissue preventing drug transport into the tumor [5,6] (Fig. 1A). Many mechanisms of intrinsic cellular chemoresistance have been reported, but a common theme has been linked to the process of epithelial-mesenchymal transition (EMT). Several studies have shown that in many solid tumors EMT is correlated with chemoresistance, tumor aggressiveness and worsened survival [7–11]. These extrinsic and intrinsic chemoresistance mechanisms can synergize and dramatically attenuate the efficacy of systemically administered drugs, resulting in the poor efficacy of systemic chemotherapy often observed in PDAC patients. There is growing evidence that overcoming such drug delivery barriers can sensitize PDAC cancer cells to conventional chemotherapies, producing a beneficial impact on patient outcomes [1–3,12]. Therefore, we hypothesized that a localized delivery approach would provide a new therapeutic option for palliative care of pancreatic cancer patients to enhance chemotherapy efficacy and reduce the intense suffering associated with their disease.

By integrating established biomaterial-science knowledge, cutting-edge technologies, computational modeling and patient-relevant cancer biology models, we engineered an implantable device that can safely deliver high concentrations of drugs inside the tumor mass to effectively inhibit tumor progression and control its dissemination in nearby vital organs. Our overall goal was to create a local delivery system for PDAC patients that could be rapidly translated into clinical practice. Consequently, we restricted our studies to FDA-approved drugs and biomaterial release systems. Poly(lactic-co-glycolic) (PLGA) is one of the most safe and well-characterized drug-eluting polymers and can be specifically modified to produce tunable local delivery platform for clinical application in pancreatic cancer settings. We first created several new patient-derived PDAC cell lines and tested their sensitivity to approved chemotherapeutic agents. After finding the cell lines were most sensitive to paclitaxel, we used a computational model to predict drug concentrations for the compound under different release scenarios. A final formulation for the paclitaxel-eluting device (PED) was obtained and we tested the efficacy of the local therapy in two orthotopic patient-derived pancreatic xenograft (PDX) mouse models with a comparison to systemic therapy. Local

therapy was superior in inhibiting tumor growth and local dissemination of the cancer cells while reducing accumulation of paclitaxel in other healthy organs, like the liver. Moreover, only local delivery of the compound was able to overcome the chemoresistance and induce large areas of necrosis within the tumor mass.

Overall, we have developed a drug-eluting device that was highly effective in treating human tumors in mice by providing increased drug concentrations inside the neoplastic lesions. The device composition provides a generalizable platform consisting of clinically approved materials that can deliver local chemotherapy to PDAC patients based on the chemosensitivity of their cancer.

This drug-eluting platform has broad implications in many solid tumors with the potential to redefine new therapeutic paradigms to treat patients with cancer. By enhancing the effect of existing chemotherapeutic agents or releasing compounds that are not currently deliverable with systemic administration, our local delivery approach has the ability to improve the quality of life and revolutionize patient outcomes by potentially converting locally advanced inoperable tumors into resectable lesions.

2. Materials and methods

2.1. Generation of patient-derived pancreatic ductal adenocarcinoma cell lines

All cell lines were generated from patients using an IRB-approved protocol 2011P001236 at the Massachusetts General Hospital. All patients signed consent for discarded tissue use for cell lines before the paracentesis procedure. One liter of discarded ascites fluid was collected from each patient and processed accordingly (See Supplementary materials). We confirmed the presence of a pure population of cancer cells after this selection method by sequencing for the *KRAS* mutation (codon 12 and 61) in the remaining cells (See Supplementary materials and Fig. S1A). Using this culture selection method we were able to establish five PDAC cell lines from different metastatic PDAC patients. These cell lines are referred to as PDAC-1, PDAC-2, PDAC-3, PDAC-5, and PDAC-6. The cell lines were characterized for proliferation and drug sensitivity *in vitro* as well as histology and orthotopic xenografts *in vivo* (See Supplementary materials).

2.2. Bioinformatics analysis of RNA sequencing data

The initial quality control of the data was carried out using the tool FASTQC. Once it was determined that the samples were good, the alignment of the samples to the reference genome was carried out using STAR aligner. The duplicate reads were marked using PICARD and removed using SAMTOOLS. The resulting BAM files were used to quantify the read counts per gene using Htseq-count program. The downstream analysis was carried out in R statistical programming language. In order to get an insight into the data, we

Fig. 1. Intrinsic and extrinsic factors determine PDAC chemoresistance. (**A**) Schematic of factors involved in PDAC chemorefractory behavior including (i) intrinsic mechanisms related to cancer cell biology and (ii) extrinsic reasons due to drug delivery barrier. (**B**) Representative pictures of H&E-stained tumor sections demonstrating different degrees of stromal deposition. Well-differentiated (PLGA-1 and -6), poorly differentiated (PDAC-2 and -3), and intermediate grade (PDAC-5) tumors are shown ("T" = tumor cells; "S" = stromal cells; Bar = 20 μm). (**C**) Unsupervised hierarchical clustering of one thousand most differentially expressed genes among all patient-derived PDAC lines. The heat map shows that PDAC-2 and PDAC-3 cluster together while PDAC-1, PDAC-5 and PDAC-6 cluster separately. (**D**) Unsupervised hierarchical clustering using an epithelial/mesenchymal gene signature (62 genes) to differentiate epithelial (CL) vs. quasi-mesenchymal (QM) and exocrine-like (EX) tumor types and cell line behavior. The heat map shows an overexpression of epithelial genes (CL) in PDAC-1, PDAC-5 and PDAC-6 while a downregulation of those genes in PDAC-2 and PDAC-3. These lines display an up-regulation of mesenchymal genes (QM). (**E**) Representative images of epithelial (CDH1, EPCAM, KRT5, KRT7, KRT8, KRT18, KRT19; *red*) and mesenchymal (FN1, CDH2, SERPINE1; *blue*) markers identified by RNA in situ hybridization staining. Epithelial tumor cells are denoted by arrowheads, while mesenchymal tumor cells are indicated by arrows (Bar = 20 μm). (**F**) Cellular migration changes demonstrated by transwell migration assay. PDAC-2 and PDAC-3 show a higher migration ability compared to the other PDAC lines. Statistically significant difference with $^*P < 0.05$, $^{**}P < 0.01$ or $^{***}P < 0.001$. (**G**) *In vitro* paclitaxel sensitivity of PDAC cell lines shown by MTT assay. (**H**) Table with the IC_{50} of all PDAC cell lines against paclitaxel, gemcitabine, fluorouracil (5-FU), oxaliplatin, irinotecan (data in **E** and **G** are displayed as mean ± standard deviation). (For interpretation of the references to colour in this figure legend, the reader is referred to the web version of this article.)

selected 100, 500, 1000 and 2000 most variant genes and did a hierarchical clustering for all samples based on the expression for these genes. The data was divided into replicates that needed to be compared for specific conditions in this case PDAC 2 and 3 clustered as one and PDAC-1, -5 and 6 as another. We used the DESEQ2 package in R for the differential expression analysis between the two clusters and to finally get a list of differentially expressed genes between any two conditions of interest. The heatmaps were plotted using the heatmap.2 function in gplots package in R.

2.3. RNA in situ hybridization (RNA-ISH)

Paraffin-embedded tissue blocks from tumor xenografts were freshly cut and frozen at $-80\,^\circ$C, then processed as described in the Supplementary materials accordingly to the Affymetrix Quanti-Gene ViewRNA ISH Tissue-2 Plex Assay.

2.4. Mathematical model of drug distribution

Time invariant rectangular tumor geometry was assumed and partitioned into three compartments, the interstitium (denoted by subscript "i"), which is assumed to be fully connected, the intra-cellular space (denoted by subscript "c") and the microvascular space (denoted by subscript "mv"). In modeling local delivery, drug efflux from the device was applied as a flux boundary condition and drug transport was calculated in the entire tissue domain. By contrast, in intravenous drug delivery each capillary within the tumor acts as a time dependent drug source, posing an intractable computational challenge. Thus, drug distribution gradients arising from intravenous delivery were only modeled in the vicinity of a single capillary. As a result, some of the equations take on slightly different forms based on the mode of drug delivery. See Supplementary materials for a detailed description of equations and parameters.

2.5. Coating of stainless steel substratum with polymeric drug-embedding matrix

We used stainless steel discs (6-mm diameter) with a 1-mm hole to allow suturing during implantation. The discs were subjected to ultrasonic cleaning in ethanol and acetone in sequence for 15 min. Two different PLGA/paclitaxel formulations were obtained, PED_10_200 and PED_20_400, that contained 10% or 20% of polymer and 200 µg or 400 µg of the drug, respectively. See Supplementary materials for detailed description.

2.6. In vitro drug release kinetics

In vitro release kinetics of Oregon Green (Life Technologies) dye-labeled paclitaxel from PED_10_200 and PED_20_400 was evaluated. A sample of each formulation was immersed in PBS and placed on a bench top orbital shaker (Thermo Scientific, Model MaxQ™ 4450) operating at 40 rpm and incubated at 37 °C. At scheduled time intervals, a sample of 50 µl was collected and replaced by fresh PBS. Collected media was analyzed by spectro-fluorimetric assay, the emission of the fluorescent label, after excitation at 488 nm, was measured at 503 nm. The linearity of the response was verified over the concentration range 0.5−250.0 µg/mL ($r^2 > 0.99$). Experiments were run in triplicate on three different batches of the synthesized polymer. Results are expressed as percentage of fluorescently-labeled paclitaxel released over time ± standard deviation.

2.7. Orthotopic xenograft mouse model, tumor burden and overall survival assessment

All animal experiments were approved by the IACUC of Massachusetts General Hospital. NOD scid gamma (NGS; NOD.Cg-Prkdcscid Il2rgtm1Wjl/Sz) mice were used for the orthotopic xenograft model. All mice were female and used between the ages of 4−6 weeks. The mice were anesthetized during the procedures (2.5% isoflurane gas). An oblique 2 cm incision (skin and peritoneal membrane) from the center of the abdomen up to the inferior left ribs was performed. 50 µl of Matrigel and DMEM (1:1) containing 100,000 cancer cells was injected into the pancreas. After injection, the abdominal cavity and skin incisions were separately closed using absorbable sutures. After two weeks for PDAC-3 and 4 weeks for PDAC-6 injected mice, the mice were divided into two groups based upon their tumor burden and delivery device was surgically implanted. Drug-delivery devices were sterilized in biosafety cabinet under UV light overnight. An oblique 2 cm incision (skin and peritoneal membrane) on top of the previous scar was performed. Tumor xenografts were identified and PED was sutured onto the tumor surface with a 4-0 absorbable suture. After delivery device implantation, abdominal cavity and skin were separately closed with two running absorbable sutures. For intravenous administration of paclitaxel, the drug was dissolved in 100% ethanol to a final concentration of 25 mg/mL. Prior to tail vein injection, 40 µl of a paclitaxel stock solution was mixed with 40 µl of Cremophor EL (1:1) and then diluted 20.8 times in a saline solution to produce a final paclitaxel concentration of 0.6 mg/ml. Mice were placed in a dedicated tail vein injection cabinet and a 1 ml syringe with 30G needle was used to inject 170 µl of the paclitaxel solution weekly (100 µg/week) to each mouse. Mouse tumors were monitored using *in vivo* luciferase imaging on the IVIS Lumina platform (Perkin Elmer/Caliper). Four weeks after PED implant the mice were given an intraperitoneal injection with 150 µl luciferin, euthanized and IVIS imaging performed for the primary tumors, peritoneal dissemination, liver and lungs. The organs were then harvested and stored for histological analysis. See Supplementary materials for more details of the methods used. Necroscopy ended by assessing tumor size and weight. In the survival experiment 12 NOD-SCID gamma mice were injected with 700000 PDAC-3 cells. After 10 days from injection, mice were randomized into two groups with homogenous tumor burden, and 5 mice were re-operated to surgically implant the PED. In parallel, mice in the control group were treated with intravenous weekly doses of paclitaxel (100 µg/week) for four consecutive weeks. Mice were sacrificed when they met the end stage criteria of our approved mouse protocol.

2.8. In vivo fluorescent drug distribution

Devices with the PED_20_400 formulation were created using Oregon Green dye-labeled paclitaxel. Devices were implanted in the NSG mice in direct contact with the tumor mass four weeks following cell injection. The control group consisted of weekly administration of fluorescent paclitaxel via tail vein injection. After two weeks of treatment, animals were sacrificed, the pancreas removed and the tissue was snap frozen in liquid nitrogen and embedded for cryosectioning. Sectioning was performed in the direction perpendicular to the delivery device placement, in order to visualize the depth of drug penetration. Slides were then washed and mounted with media containing propidium iodide to stain the nuclei. Confocal imaging was performed in the green (drug) and red (nuclei) channels using a Zeiss LSM 510 (Confocal Core Facility at the Beth Israel Deaconess Medical Center, Harvard Medical School, Boston, MA) and Nikon A1R Ultra-Fast Spectral Scanning Confocal Microscope (Koch Institute Swanson Biotechnology Center,

Cambridge, MA). Multiple images were taken to create z-stacked images and reconstructed using the microscope software (Zeiss). The software was used to determine the green intensity profiles along a selected line in order to analyze depth of drug penetration.

3. Results

3.1. Intrinsic and extrinsic factors that determine PDAC chemoresistance

To design a local therapy relevant to human pancreatic cancer, we generated five patient-derived cell lines by culturing the ascites fluid from patients with metastatic pancreatic cancer. The cancer origin was confirmed by *KRAS* gene mutation sequencing matched to the initial diagnostic biopsy (see SI Appendix and Fig. S1A). These newly established PDAC lines were orthotopically injected into immunodeficient mice to demonstrate tumorigenicity of all cell lines (Fig. S1B). Histological analysis of the tumor xenograft revealed a spectrum of high grade, undifferentiated morphology in PDAC tumors generated from lines PDAC-2 and PDAC-3, while tumors from PDAC-1 and PDAC-6 exhibited a differentiated morphology with gland-forming ability and notable stromal deposition. PDAC-5 was in the middle of this spectrum and showed an intermediate grade tumor and PDAC-6 produced the highest desmoplastic stromal reaction (Fig. 1B). Thus, these lines provided a range of pancreatic cancer properties, representing the heterogeneity inherent in patient disease.

To better characterize the different phenotypes observed from these cell lines, RNA-sequencing was performed on the tumor lines. Unsupervised clustering of gene expression profiles recapitulated the similarities among cell lines previously categorized by their histological differences (Fig. 1C). Differential expression analysis of the two groups of cell lines revealed increased expression of mesenchymal genes in PDAC-2 and PDAC-3 when compared to PDAC-1, PDAC-5, and PDAC-6 (Fig. S1C). We then applied a 62 gene set [13] previously shown to separate PDAC tumors and cell lines into three different subtypes including exocrine-like, classical, and quasi-mesenchymal. Consistent with our global RNAseq analysis, we found that PDAC-1, PDAC-5 and PDAC-6 to have a classical epithelial phenotype while PDAC-2 and PDAC-3 had a quasi-mesenchymal expression signature (Fig. 1D). These differences in classical epithelial and quasi-mesenchymal gene expression signatures were maintained *in vivo* as seen in patient-derived xenograft (PDX) tumor stained for epithelial and mesenchymal markers [14] with RNA in situ hybridization (Fig. 1E).

Paralleling the differences in transcriptional signatures, PDAC-2 and PDAC-3 had faster proliferation rates and higher migration through trans-well chambers compared to the more well-differentiated PDAC lines, PDAC-1 and PDAC-6 (Fig. 1F, see Supplementary materials and Fig. S1E). To further characterize differences in key EMT markers at the protein level, we performed a western blot assay of the classic epithelial marker E-cadherin (CDH1) and mesenchymal marker Vimentin (VIM) (Fig. S1F). Notably, we found that PDAC-3 is the only pancreatic line that has significant loss of E-cadherin and acquisition of Vimentin at the protein level. This indicates that even though PDAC-2 and PDAC-3 share many quasi-mesenchymal features, E-cadherin and Vimentin protein status are significantly different.

We then tested the intrinsic drug resistance of our patient-derived cell lines to known active chemotherapeutic agents in pancreatic cancer treatment (Fig. 1G, Supplementary materials and Fig. S1G). All cell lines showed significant chemoresistance to single agent 5-fluorouracil, oxaliplatin, and irinotecan. There was striking single agent activity of gemcitabine and paclitaxel at nanomolar (nM) concentrations in PDAC-1, PDAC-2, and PDAC-6

(Fig. 1H and Supplementary materials). The PDAC-5 cell line had intermediate sensitivity to these agents, but notably, PDAC-3 had significantly increased multi-drug resistance compared to the other patient derived cell lines. Given the differences in PDAC-2 and PDAC-3 sensitivity to chemotherapy despite shared quasi-mesenchymal features, we hypothesized that the differences in EMT proteins confer intrinsic chemoresistance not found in RNA-seq data. Indeed, the western blot of the classic epithelial marker E-cadherin (CDH1) and mesenchymal marker Vimentin (VIM) revealed PDAC-3 had much lower E-cadherin and higher Vimentin compared to all other cell lines including PDAC-2. Interestingly, PDAC-5 also had diminished E-cadherin levels, albeit not as much as PDAC-3, and was also found to be the second most resistant cell line to paclitaxel. This is consistent with previous work indicating that quasi-mesenchymal cell lines are generally more chemo-resistant [13]. Together, this suggests that EMT marker protein status may be a better predictor of chemosensitivity than the other characteristics.

Interestingly, paclitaxel had the most activity across all cell lines, including PDAC-3, outperforming even gemcitabine, the only single agent with demonstrated efficacy in humans (Fig. 1H). The combination of paclitaxel efficacy across these cell lines and the known difficulty in delivering this compound systemically, supported the merit of developing a paclitaxel localized therapy platform for PDAC. We selected the PDAC-3 cell line for its intrinsic chemo-resistant behavior and PDAC-6 for its robust stromal reaction to cover the spectrum of PDAC extrinsic and intrinsic chemoresistance in our *in vivo* experimental models.

3.2. Systemic chemotherapy fails to deliver the agents to the tumor core

We developed a computational model to examine the role of transport barriers in resistance to chemotherapy by predicting the spatiotemporal dynamics of paclitaxel distribution in PDAC-3 tumor tissue after intravenous (I.V.) administration of chemotherapy. The focus on paclitaxel distribution was dictated by its enhanced efficacy against all cell lines tested and the steepest dose response curve. A compilation of computational modeling transport parameters is provided in Supplementary materials Tab. S1 and S2. Model simulations predict that intravenous delivery of paclitaxel provides limited spatial distribution over time (Fig. 2A, Supplementary Materials Movie S1), with a peak drug concentration of 12 μM and a rapid decay from the blood capillaries (Fig. 2B), reinforcing the assertion that standard-of-care systemic treatment fails to deliver the drug at significant concentrations within the tumor. This indicates that the IC_{50} of intravenous paclitaxel would only be reached in the region immediately surrounding the tumor vasculature. To verify the *in vivo* relevance of these computational predictions, we quantified the distribution of fluorescently-labeled paclitaxel inside PDAC-3 orthotopic patient-derived xenograft two hours post intravenous administration [15]. Consistent with matching model predictions, confocal images of tissue sections showed localized patterns of fluorescently-labeled drug that sparse the microvasculature (Fig. 2C). Quantitative image analysis confirmed that paclitaxel merely penetrated up to 10 μm from the vascular source (Fig. 2D). Linear scan analysis revealed only a very limited amount of the drug actually present in the tissue (Fig. 2E). These results demonstrate the predictive power of the computational model and highlight the major limitations of delivering paclitaxel intravenously due to the tumors desmoplastic effects and hypovascularity.

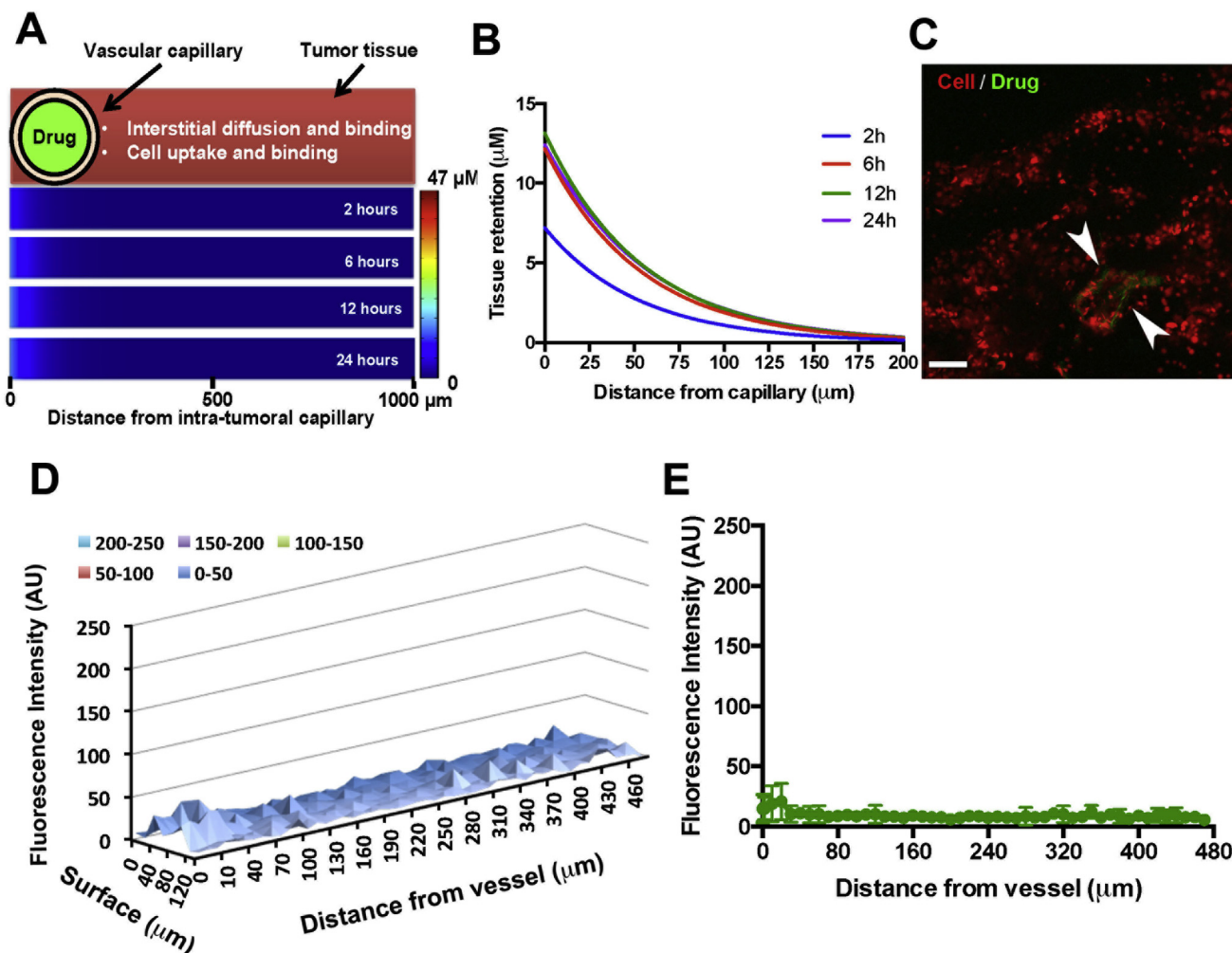Supplementary data related to this article can be found online at http://dx.doi.org/10.1016/j.biomaterials.2016.03.044.

Fig. 2. Computational modeling of drug delivery to pancreatic tumors. (**A**) Layout of the computational domain consisting of a single vascular capillary (in pink) from which intravenously delivered drug (green) is transported into the surrounding tumor tissue (red) and distributes via interstitial diffusion/binding and cell uptake/binding. Underneath is represented the presence of drug over a time course of 24 h within the tumor mass. (**B**) Linear representation of tissue distribution predicts that drug will reach tumor site at a very limited concentration. (**C**) Confocal imaging of a tumor tissue section after 14 days treatment consisting of weekly injection of paclitaxel-Cremophore formulation. Image taken two hours after intravenous injection highlights presence of the fluorescent paclitaxel only at the lumen/tissue interface (Bar = 100 μm). (**D**) Analysis of the fluorescence intensity at the surface. (**E**) Fluorescence intensity are in accordance with computational prediction of very limited drug penetration (data shown are displayed as mean ± standard deviation). (For interpretation of the references to colour in this figure legend, the reader is referred to the web version of this article.)

3.3. Design of an implantable drug delivery platform for local therapy

To overcome the systemic delivery barrier introduced by fibrosis surrounding the tumor and lack of vasculature, we developed a biodegradable polymer based drug-eluting device for localized delivery of chemotherapeutic agents. We tested this device in comparison to intravenous therapy using a patient-derived xenograft mouse model (Fig. 3A). Guided by our computational model and considerations required for surgical implantation, we designed a mouse-size paclitaxel eluting device (PED) as a poly(lactic-co-glycolic) acid (PLGA) matrix embedded with paclitaxel adhered onto a 316L stainless steel disc. This setting allowed us to accurately investigate polymer-metal interface, adhesion, degradation and release kinetics. We tested two different formulations, PED_10_200 and PED_20_400, differing from one another by PLGA concentration and paclitaxel amount. Both systems were fully characterized (see Supplementary materials and Fig. S2A), and surface chemical analysis confirmed the presence of polymeric atomic elements at the expected stoichiometric ratio (see Supplementary materials and Fig. S2B–C). Morphological examination of both formulations

revealed a smooth surface without cracks or bubbles (Fig. 3B) and a uniform thickness across all measured locations as determined by environmental scanning electron microscopy (Fig. 3C). Polymer thickness is highly important due to its direct relationship to the PLGA degradation kinetics, and therefore to the elution rate of paclitaxel. The hydrolytic bulk degradation of the polymer requires the surrounding fluids to imbibe the coating layer, triggering bulk degradation [16] and initiating drug release without generating dangerous superficial cracks that can be seen in other polymer systems. *In vitro* incubation in aqueous media allowed us to verify significant adherence to the metallic substratum and homogenous degradation, as shown by the presence of a hydrated coating at later time points (Fig. 3D).

The PLGA-based drug release formulations are dependent on polymer degradation, and affected by shape, polymer, drug ratio, and the mechanism of hydrolysis [17–19]. We achieved sustained release of fluorescently-labeled paclitaxel for more than one month from both PED_10_200 and PED_20_400 devices. We successfully created a platform technology where the release kinetics can be accurately tuned using different ratios of PLGA and paclitaxel.
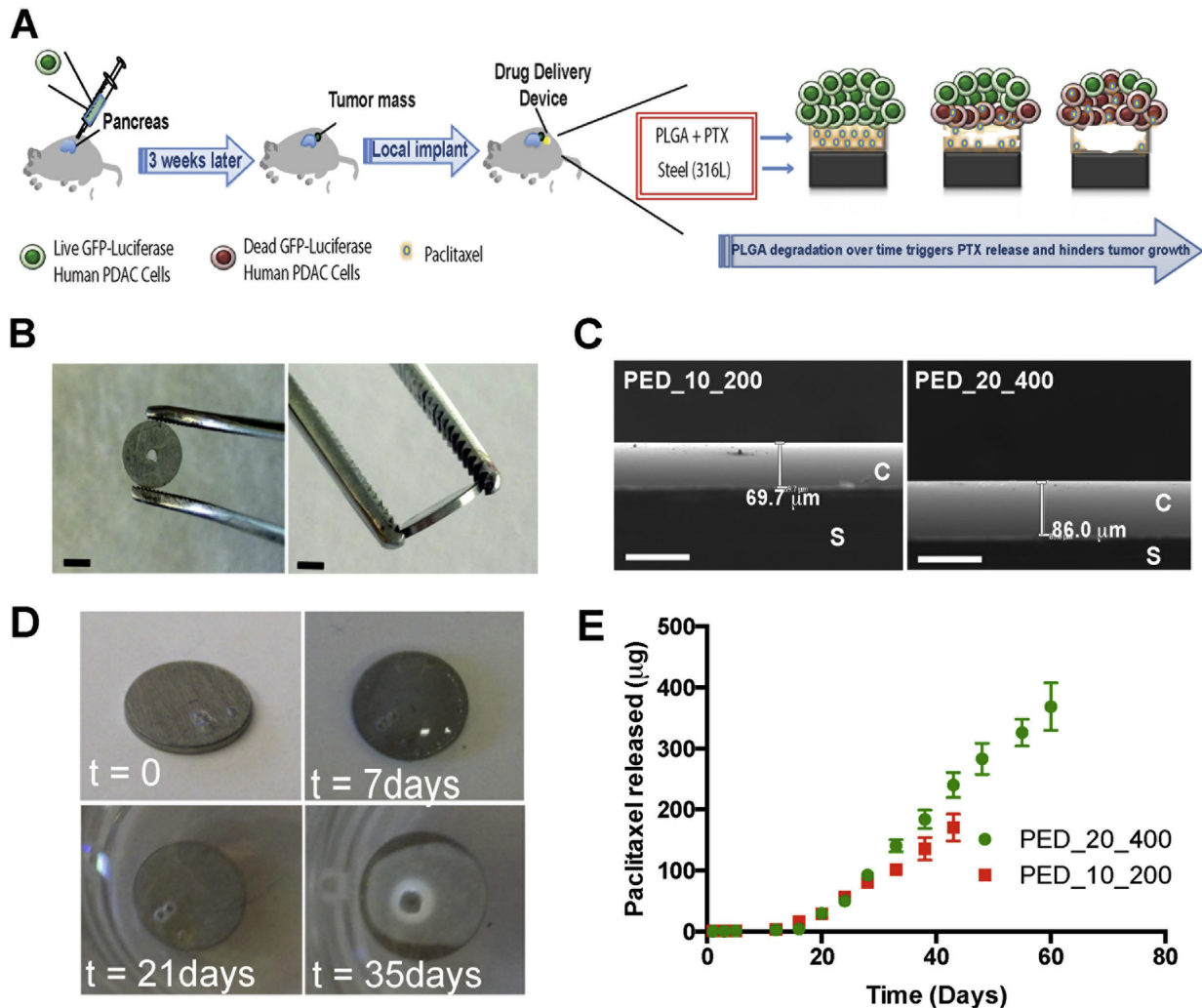
Fig. 3. Design and characterization of an implantable paclitaxel eluting device. (**A**) Schematic of localized therapeutic approach with a paclitaxel eluting device (PED). (**B**) Macroscopic visualizations of the local delivery device (Bar = 3 μm). (**C**) Evaluation of coating thickness using scanning electron microscopy (Bar = 100 μm). Coating methodology ensured a platform technology with similar outcomes for two different formulations differing in PLGA amount (10% and 20% respectively) and paclitaxel loading (200 μg or 400 μg respectively; "C" = coating and "S" = steel). (**D**) Characterization of degradation of the coatings. Bulk polymeric degradation was homogeneous and without superficial cracks. (**E**) *In vitro* linear release kinetics showed tunable delivery for over a month from both formulations with adjustable therapeutic dose (data are displayed as mean ± standard deviation).

Furthermore, the two delivery devices are designed to release different amounts of chemotherapeutic agent with similar kinetics (Fig. S2D). By doubling both the drug content and polymer concentration, we were able to tune the formulations to accomplish a linear release of paclitaxel, which boosted the effective dose and increased the length of *in vitro* release from 45 days (PED_10_200) to 60 days (PED_20_400) (Fig. 3E). An additional consideration is that the inflammation at the site of implantation following stenting or any other procedure is very common and the release of a chemotherapeutic drug too early may result in harmful complications by preventing healing. To address this issue, we modified the polymer concentration engineering a delay in drug release between 10 and 17 days, allowing time for the surgical wounds to heal before chemotherapy began.

3.4. Local therapy enhances intratumoral drug distribution

The rationale behind our strategy was to demonstrate that local therapy would allow for higher intratumoral paclitaxel distribution and cytotoxicity compared to intravenous administration. Computational modeling predicted that the release kinetics achieved by the PED_20_400 device (Supplementary materials and Fig. S2E) should provide markedly improved intratumoral paclitaxel distribution with increased drug concentration by day 3, and extend over a prolonged period of time to reach tissue concentrations as high as 45 μM (Fig. 4A, Supplementary materials Movie S2). Moreover, linear plots forecasted a depth of penetration as high as 1000 μm after 30 days of treatment (Fig. 4*B*).

Supplementary data related to this article can be found online at http://dx.doi.org/10.1016/j.biomaterials.2016.03.044. To evaluate the computational prediction of significantly higher delivery of paclitaxel deep into the tumor core at cytotoxic concentrations, we recapitulated the experiment in mice bearing delivery devices with fluorescently-labeled paclitaxel to measure drug distribution inside PDAC-3 pancreatic PDX tumors. Two weeks after implantation, the tumors demonstrated deposition of fluorescent paclitaxel when observed under a dissecting microscope (Fig. 4C). To quantify intratumoral drug penetration, serial sections were taken from the tumor perpendicular to the delivery device and were imaged using confocal microscopy (see Supplementary materials and Fig. S2F). The paclitaxel distribution in the local delivery device group had markedly increased drug concentration within the tumor in
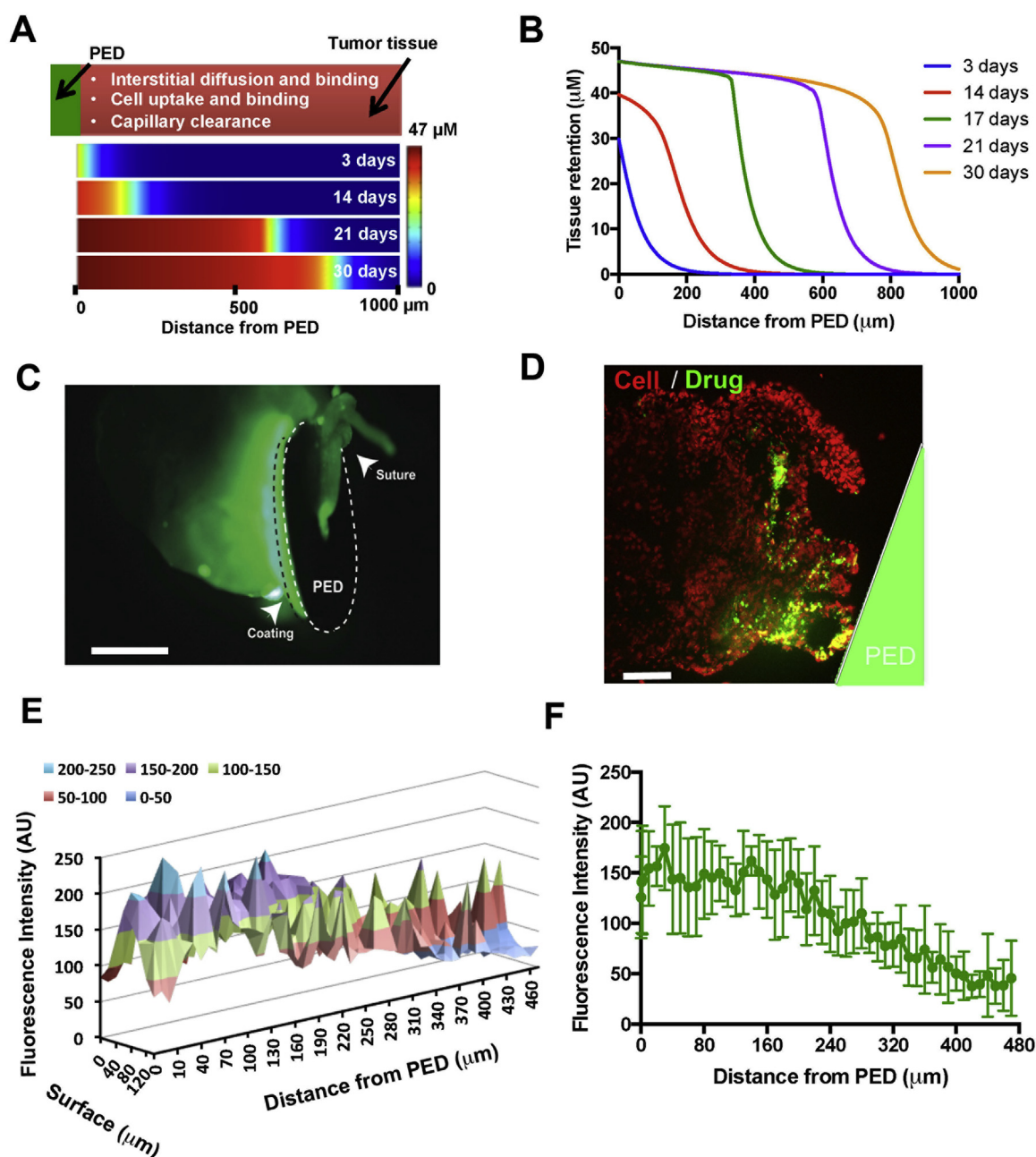
Fig. 4. Localized therapeutic strategy implementing PED greatly enhances intratumoral deliverability of chemotherapeutic agents. (**A**) Schematic of the computational domain consisting of a confined tumor tissue (red), the device as source of drug (green) taking into consideration interstitial diffusion/binding, cell uptake/binding and capillary clearance. Underneath is represented drug distribution over a course of 30 days within the tumor mass. (**B**) Linear representation of intratumoral drug distribution predicts elevated paclitaxel tissue retention as a function of release kinetics and extended over 1 mm after 30 days of treatment. (**C**) Representative fluorescent image under a dissecting microscope of tumor mass harvested 14 days post-treatment points out a macroscopic drug presence (Bar = 3 μm). (**D**) Confocal analysis of tumor tissue sections highlight the extensive penetration of the drug at increased distance form the tumor/PED interface (Bar = 100 μm). Image represents a time point of 14 days post-implant of the PED. (**E**) Surface analysis and (**F**) Fluorescent intensity from tissue was in accordance with computational predictions of drug penetration after 14 days of treatment (data in are displayed as mean ± standard deviation). (For interpretation of the references to colour in this figure legend, the reader is referred to the web version of this article.)

comparison to intravenous dosing (Figs. 4D and 2C). The local drug delivery achieved a qualitatively different distribution pattern with high drug deposition spanning over 140 μm of the surface at the tumor/device interface (Fig. 4E–F). Paclitaxel penetration depth extended over 400 μm from the delivery device, in perfect accordance with the prediction of the computational model at 14 days, a result that was 40-fold deeper than what was achieved with intravenous administration (Fig. 4F versus intravenous concentration shown in Fig. 2E). Together, these results demonstrate that

local delivery of high payloads of anti-neoplastic agents can overcome the transport barriers that impede adequate distribution following systemic administration (Supplementary materials and Fig. S2G–H).

We took advantage of fluorescently-labeled paclitaxel to also detect drug distribution inside mouse organs and within tumor xenografts. We demonstrated that drug is differentially distributed between primary tumors and mouse organs in systemic versus localized treatment (Fig. S2I). Specifically, in mice-bearing PED,

paclitaxel retention inside the xenografts tumors is significant higher (6.5 times) compared to distal organs (5.2 ± 0.1 fluorescent signal/millisecond in tumor xenografts vs. 0.8 ± 0.4 fluorescent signal/millisecond in distal organs). This highlighted the modest exchange of paclitaxel between pancreatic tumors and mouse circulation. These data are in accord with the potential of reducing the high systemic side effects and organ toxicity present with many chemotherapy treatments. Moreover, tumor xenografts in IV mouse group have 3.9 times lower concentrations of paclitaxel compared to PED-treated tumors (1.3 ± 0.5 fluorescent signal/millisecond in IV treated mice vs. 5.2 ± 0.1 fluorescent signal/millisecond in PED-treated mice). All together, these results are indicative of minimal systemic distribution of paclitaxel when locally delivered from PED, which can potentially limit the systemic side effects of compounds in PDAC patients.

3.5. Local therapy has enhanced efficacy for treatment of pancreatic tumor xenografts

To test efficacy of our local approach, mice were injected with luciferase-expressing pancreatic cancer lines to create orthotopic tumors. We investigated the PDAC-3 cell line as a model of intrinsic chemoresistant behavior and the PDAC-6 cell line as a model of extrinsic chemoresistance through development of a desmoplastic stromal barrier. After 2 or 4 weeks following the injection with PDAC-3 or PDAC-6 cells, the mice were randomized into two treatment groups with systemic therapy or local delivery of paclitaxel (Fig. S3A). The design of the local delivery device allowed for direct surgical implantation and fixation to the tumor using standard surgical sutures to avoid any issues of device migration or off target delivery. The control group was treated with equivalent total dose of paclitaxel through intravenous injection given weekly for 4 weeks (Fig. 5A). Safety of the device was determined by weekly examinations of mice bearing the local delivery device. All mice survived surgical implantation, and none showed any detectable postoperative complications.

In vivo efficacy was assessed by comparing the tumor burden with the local delivery device versus mice treated with an intravenous injection of paclitaxel. Tumor burden was assessed by bioluminescence imaging during treatment, and by measuring *ex vivo* the pancreatic tumor volumes and mass. Both PDAC-3 and PDAC-6 PDX tumors responded significantly more to local delivery of paclitaxel compared to the systemic regimen. After a month of treatment, we observed a 12-fold and 2-fold average reduction of viable tumor volume by *in vivo* luciferase imaging in respective PDAC-3 and PDAC-6 tumors in mice with the local delivery device compared to mice treated with intravenous paclitaxel (Fig. 5B–C). Furthermore, mice treated with the local delivery device presented both lower pancreatic tumor mass and volume (Fig. 5D–F, Supplementary materials and Fig. S3B) compared to control mice. Necropsy examinations macroscopically confirmed the absence of any injuries to abdominal organs surrounding the local delivery device and the absence of device displacement within the peritoneal cavity (Supplementary materials and Fig. S3C). Histological analysis of the xenograft tumors showed preserved tumor architecture in animals exposed to intravenous paclitaxel, while massive areas of necrosis were seen in tumors treated with the PED (Fig. 5G). Systemic toxicity of PED was ruled out by carefully assessing organ integrity during mouse autopsy, and by reviewing with a pathologist blinded to specimen treatment hematoxylin and eosin tissue slides obtained from muscle, lung, liver, ovary, kidney and spleen of mice-bearing PED to confirm a normal organ architecture (Fig. 5H).

These results combined with our viable tumor assessment by luciferase-based imaging indicate that the measurable effects of localized therapy are greater than the reduction in total tumor size alone given the substantial contribution of necrotic non-viable cells in the tumor mass. Moreover, we found better control of local tumor dissemination in mice-bearing PDAC-6 tumors treated with the local delivery device compared to mice treated with equivalent doses of intravenous paclitaxel (Fig. 5I; Supplementary materials).

To test whether the higher response to treatment of the localized delivery approach would have a favorable impact on overall survival, we performed an additional *in vivo* experiment using PDAC-3 line. We observed a 28-day increase in the median overall survival of mice treated with PED compared to mice treated with a systemic regimen of paclitaxel (Fig. 5J, p = 0.0015), increasing life expectancy in our model.

Altogether, our results demonstrate the ability to control pancreatic cancer progression in terms of tumor growth, local dissemination, and survival when a local delivery approach is used over a traditional systemic delivery.

4. Discussion

Over the last 40 years, systemic chemotherapies have been shown to be largely ineffective in pancreatic cancer. A plethora of strategies have been implemented for improving drug delivery — including, liposome formulations [20] and proteins as natural biomaterials to stabilize drug deliverability [21]. These studies showed some promising results although they still rely on systemic delivery and its limitation. Using a biodegradable PLGA polymer, we developed a highly tunable multi-purpose drug-eluting device to deliver elevated payloads of chemotherapeutic agents that can be locally released to reach higher intratumoral concentrations not achievable by systemic administration. By means of fluorescently-labeled paclitaxel, we demonstrated significantly increased tissue penetration of drug using the local delivery device compared to systemic intravenous dosing. The choice of the optimal material for drug delivery formulations is dictated by the simultaneous presence of the following characteristics: *i.* Homogenous mixture of polymer and drug, to ensure spatial control of drug release; *ii.* Inert polymer-solvent-drug interactions, to protect pharmacological activity; and *iii.* Compatibility of matrix preparation methods with manufacturing techniques for successful translation into the clinic.

To enhance clinical translation, our choice of materials and drugs was restricted to FDA-approved compounds. In prior work, another group had created a pancreatobiliary drug eluting stent using a polyurethane material that was shown to be safe for humans [22–24]. However, the efficacy was not achieved, potentially due to limited transport of the drug to the primary tumor from the biliary system and the lack of controlled polymer erosion to obtain adequate sustained drug release. Our approach of creating a device that can be used to wrap the tumor/biliary duct has the advantage of allowing greater material delivery, removing exposure the biliary flow that may cause drug washout and facilitating patient specific delivery of the drug tailored to the individual's tumor burden. The PLGA-coated device ensured reliable and predictable *in vivo* release kinetics that are tailor-designed to match the specific anatomical position and requirement of PDAC with release delayed for at least 7 days to allow for effective wound healing followed by a sustained constant elution for at least two months. In our studies, this continuous delivery of high drug concentration was achievable without any adverse effects to the animals and with a notable reduction of viable tumor cells of two different PDAC patient-derived xenografts. It's worth to notice, the hypovascularity of the tumor mass, major barrier of systemic delivery, ensures high retention within the tumor mass in the case of local delivery by hindering the leak of the drug into the circulation. Thus we transform one of the bigger limitations of systemic administration in
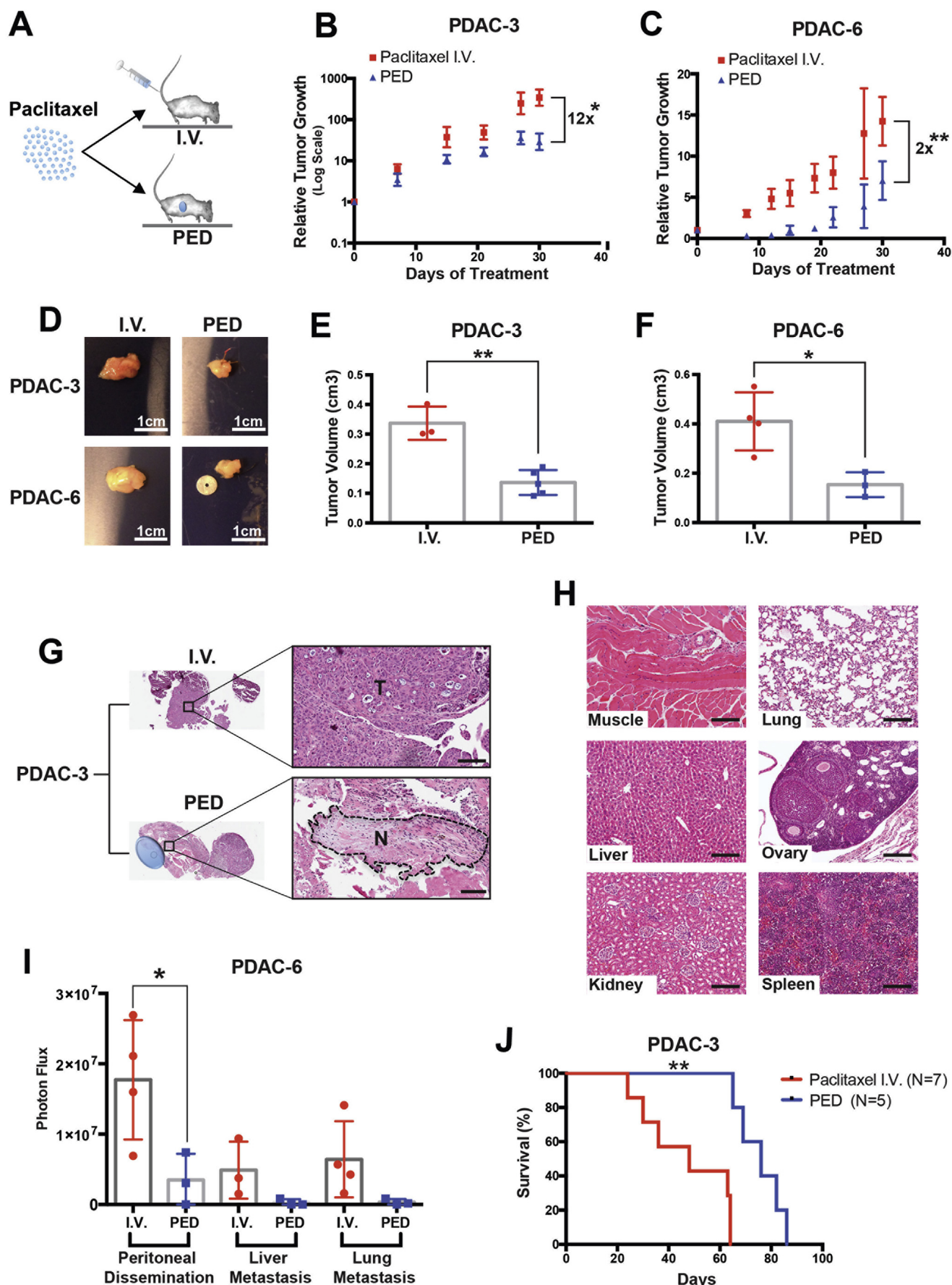
pancreatic cancer into a strength for a localized approach.

The results obtained in our study provide proof-of-principle that effective local delivery of conventional cytotoxic agent can overcome intrinsic and extrinsic chemoresistance mechanisms, opening new therapeutic strategies to improve the outcomes of PDAC patients. Notably, similar to our *in vitro* testing, paclitaxel is efficacious when enhanced systemic delivery vehicles are employed [25–27]. The albumin nanoparticle encapsulated paclitaxel system (nab-paclitaxel) was shown to be effective in combination with gemcitabine in a randomized phase III trial [28], though response rates were only modestly improved to 23% versus 7% with a survival benefit of 1.8 months. These effects may be due to improved tolerability of nab-paclitaxel or longer half-life in circulation as demonstrated in a mouse model [29]. Our results suggest that even greater on-target cytotoxicity can be achieved by delivering agents like paclitaxel directly to the tumor resulting in dramatically increasing overall median survival of more than 50% following improved response rates and decreased side effect profiles. Furthermore, we showed that this platform can help to control local tumor invasion, acting as a physical barrier, which would potentially translate to better palliation of symptoms related to bile duct occlusion and local invasion into surrounding tissues and vital organs.

To successfully propel a local delivery approach from the bench to the clinic, it is important to provide the physicians with a flexible drug-eluting platform that can be tuned to the PDAC patients. The approach tested in these studies is highly adaptable in its use and application. It can be fabricated in virtually any shape with tailorable release kinetics and can be easily adapted to several therapeutic strategies (Fig. 6). For instance, the local delivery device can be applied to a flexible, rather than metallic, substrate with the polymeric formulation to create a foldable, completely biodegradable, multi-organ drug-eluting platform (Fig. 6, Drug Delivery Matrix − DDM). A translation of our mouse-size drug-eluting device for humans could be implanted during an open or laparoscopic surgical procedure directly in contact with the tumor. This may provide a strategy to enhance neoadjuvant treatments in unresectable locally advanced tumors with the potential to increase the survival of these patients, which currently is less than 12 months [30–32]. Another application would be to assemble the PLGA matrix with a rigid tubular plastic/metal substrate as a novel pancreatobiliary stent-based drug release platform (Fig. 6, Drug Releasing Stent − DRS). This would provide both mechanical support for the ductal system and release high concentrations of chemotherapy into the compressing tumor. This may lead to a significant increase in the longevity of the stent, which would improve our ability to palliate biliary obstruction symptoms, reduce the number of re-stenting procedures, and improve the quality of life in patients with both pancreatic and bile duct cancers.

5. Conclusions

Overall, the results obtained in our study are a proof-of-principle that local drug delivery platform can effectively
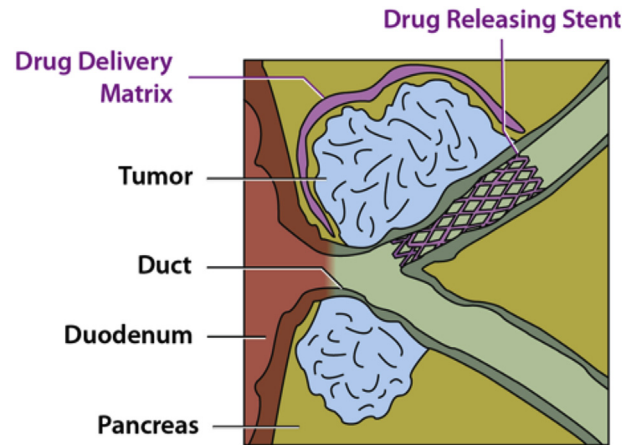

Fig. 6. Schematic layout of different types of device and approach. Fully biodegradable Drug Delivery Matrix (DDM) inserted via minimal invasive laparoscopic surgery cages the tumor, controlling invasion in nearby organs, and locally releases the agent increasing efficacy of treatment. Drug Releasing Stent (DRS) implanted through ECR relieves blockage of the bile duct and locally releases the agent increasing efficacy of treatment.

overcome intrinsic and extrinsic PDAC chemoresistance, opening the door for novel strategies to treat patients with pancreatic cancer. By implanting a local drug-eluting device, we could improve the survival of patients with locally advanced tumors, who currently have a life expectancy of several months, and the quality of life of metastatic patients, who suffer from debilitating symptoms caused by local tumor infiltration. All of these advantages are relevant to many locally advanced inoperable solid tumors. From an initial basis in pancreatic cancer this approach can therefore be expanded to other types of cancer like colorectal cancer, and has the potential to resuscitate several drugs that have been shelved after clinical trials because of inadmissible systemic toxicity. In conclusions, our target delivery platform addresses a clinical problem affecting the majority of cancer patients and provides the mechanistic insight to drive this concept to the clinic safely, effectively and rapidly.

Fig. 5. Response to treatment is highly improved by targeted delivery of chemotherapy. (**A**) Schematic representation of the *in vivo* model design used to compare the efficacy of paclitaxel delivered intravenously (intravenous) to the paclitaxel eluting device (PED) treatment. (**B-C**) Relative tumor growth curves of PDAC-3 and PDAC-6 mouse xenografts after either paclitaxel intravenous or PED treatment (data are displayed as mean ± s.e.m). (**D**) Representative images of tumor masses isolated from PDAC xenografts after treatment with intravenous or locally delivered paclitaxel. (**E-F**) Tumor volume of PDAC xenografts after treatment with intravenous or locally-delivered paclitaxel (data are displayed as mean ± standard deviation). (**G**) Histological analysis of the tumor showing areas of necrosis (N) in tumors treated with locally delivered paclitaxel compared to preserved tumor architecture (T) in mice treated with intravenous paclitaxel (bar = 100 μm). (**H**) Representative images of different organs of mice treated with PED. The histological tissue sections show intact organ architecture without any area of necrosis (hematoxylin and eosin staining, bar = 150 μm). (**I**) Graph showing reduction of the local peritoneal dissemination in PDAC-6 injected mice that were treated with local delivery device compared to systemic administrations of paclitaxel. *Statistically significant difference with $p < 0.05$. **Statistically significant difference with $p < 0.01$. (**J**) Kaplan-Meier curves showing a significant 28-day increase in the median overall survival of mice treated with PED compared to mice treated with paclitaxel I.V. (**$p = 0.0015$).

Appendix A. Supplementary data

Supplementary data related to this article can be found at http://dx.doi.org/10.1016/j.biomaterials.2016.03.044.

Author contribution

L.I., D.T.T., E.R.E, M.L conceived, designed and oversaw all of the studies; L.I., M.L., D.T.T., K.X., F.B., and N.A. performed the experiments; V.D. reviewed all pathology, A.R.T. performed the computational experiments and V.T. the bioinformatic analysis. E.R.E., R.L., J.W.C., A.B.B., C.R.F., and D.A.H. reviewed the data and provided input; L.I., D.T.T., M.L., A.B.B., E.R.E. wrote the paper, which all authors edited.

Disclosure

L.I., M.L., D.T.T., C.R.F., J.W.C., R.L. E.R.E. are inventors in a patent application based on this technology.

References

[1] K.P. Olive, et al., Inhibition of Hedgehog signaling enhances delivery of chemotherapy in a mouse model of pancreatic cancer, Science 324 (5933) (2009) 1457–1461.
[2] A. Neesse, et al., Stromal biology and therapy in pancreatic cancer, Gut 60 (6) (2011) 861–868.
[3] C. Feig, et al., The pancreas cancer microenvironment, Clin. Cancer Res. 18 (16) (2012) 4266–4276.
[4] P.P. Provenzano, et al., Enzymatic targeting of the stroma ablates physical barriers to treatment of pancreatic ductal adenocarcinoma, Cancer Cell 21 (3) (2012) 418–429.
[5] A. Sofuni, et al., Differential diagnosis of pancreatic tumors using ultrasound contrast imaging, J. Gastroenterol. 40 (5) (2005) 518–525.
[6] H. Sakamoto, et al., Utility of contrast-enhanced endoscopic ultrasonography for diagnosis of small pancreatic carcinomas, Ultrasound Med. Biol. 34 (4) (2008) 525–532.
[7] S. Dangi-Garimella, S.B. Krantz, M.A. Shields, P.J. Grippo, H.G. Munshi, Epithelial-mesenchymal transition and pancreatic cancer progression, in: Pancreatic Cancer and Tumor Microenvironment, Grippo PJ & Munshi HGTrivandrum, India, 2012.
[8] Z.A. Rasheed, et al., Prognostic significance of tumorigenic cells with mesenchymal features in pancreatic adenocarcinoma, J. Natl. Cancer Inst. 102 (5) (2010) 340–351.
[9] Z. Wang, et al., Acquisition of epithelial-mesenchymal transition phenotype of gemcitabine-resistant pancreatic cancer cells is linked with activation of the notch signaling pathway, Cancer Res. 69 (6) (2009) 2400–2407.
[10] T. Arumugam, et al., Epithelial to mesenchymal transition contributes to drug resistance in pancreatic cancer, Cancer Res. 69 (14) (2009) 5820–5828.
[11] A.N. Shah, et al., Development and characterization of gemcitabine-resistant pancreatic tumor cells, Ann. Surg. Oncol. 14 (12) (2007) 3629–3637.
[12] A. Neesse, et al., CTGF antagonism with mAb FG-3019 enhances chemotherapy response without increasing drug delivery in murine ductal pancreas cancer, Proc. Natl. Acad. Sci. U. S. A. 110 (30) (2013) 12325–12330.
[13] E.A. Collisson, et al., Subtypes of pancreatic ductal adenocarcinoma and their differing responses to therapy, Nat. Med. 17 (4) (2011) 500–503.
[14] M. Yu, et al., Circulating breast tumor cells exhibit dynamic changes in epithelial and mesenchymal composition, Science 339 (6119) (2013) 580–584.
[15] A. Sparreboom, O. van Tellingen, W.J. Nooijen, J.H. Beijnen, Nonlinear pharmacokinetics of paclitaxel in mice results from the pharmaceutical vehicle Cremophor EL, Cancer Res. 56 (9) (1996) 2112–2115.
[16] M. Biondi, et al., Bioactivated collagen-based scaffolds embedding protein-releasing biodegradable microspheres: tuning of protein release kinetics, J. Mater. Sci. Mater. Med. 20 (10) (2009) 2117–2128.
[17] L. Indolfi, et al., Microsphere-integrated drug-eluting stents: PLGA microsphere integration in hydrogel coating for local and prolonged delivery of hydrophilic antirestenosis agents, J. Biomed. Mater. Res. A 97 (2) (2011) 201–211.
[18] D.N. Kapoor, et al., PLGA: a unique polymer for drug delivery, Ther. Deliv. 6 (1) (2015) 41–58.
[19] F. Ungaro, et al., Microsphere-integrated collagen scaffolds for tissue engineering: effect of microsphere formulation and scaffold properties on protein release kinetics, J. Control Release 113 (2) (2006) 128–136.
[20] A. Wang-Gillam, et al., Nanoliposomal Irinotecan with Fluorouracil and Folinic Acid in Metastatic Pancreatic cancer after Previous Gemcitabine-based Therapy (NAPOLI-1): a Global, Randomised, Open-label, Phase 3 Trial, Lancet, 2015.
[21] M. Al-Hajeili, A.S. Azmi, M. Choi, Nab-paclitaxel: potential for the treatment of advanced pancreatic cancer, Onco Targets Ther. 7 (2014) 187–192.
[22] K.T. Suk, et al., Human application of a metallic stent covered with a paclitaxel-incorporated membrane for malignant biliary obstruction: multicenter pilot study, Gastrointest. Endosc. 66 (4) (2007) 798–803.
[23] D.K. Lee, et al., The effect on porcine bile duct of a metallic stent covered with a paclitaxel-incorporated membrane, Gastrointest. Endosc. 61 (2) (2005) 296–301.
[24] S.I. Jang, et al., Efficacy of a metallic stent covered with a paclitaxel-incorporated membrane versus a covered metal stent for malignant biliary obstruction: a prospective comparative study, Dig. Dis. Sci. 58 (3) (2013) 865–871.
[25] D.A. Yardley, nab-Paclitaxel mechanisms of action and delivery, J. Control. Release Off. J. Control. Release Soc. 170 (3) (2013) 365–372.
[26] D.D. Von Hoff, et al., Gemcitabine plus nab-paclitaxel is an active regimen in patients with advanced pancreatic cancer: a phase I/II trial, J. Clin. Oncol. 29 (34) (2011) 4548–4554.
[27] J.M. Lohr, et al., Cationic liposomal paclitaxel plus gemcitabine or gemcitabine alone in patients with advanced pancreatic cancer: a randomized controlled phase II trial, Ann Oncol. 23 (5) (2012) 1214–1222.
[28] D.D. Von Hoff, et al., Increased survival in pancreatic cancer with nab-paclitaxel plus gemcitabine, N. Engl. J. Med. 369 (18) (2013) 1691–1703.
[29] A. Neesse, et al., SPARC independent drug delivery and antitumour effects of nab-paclitaxel in genetically engineered mice, Gut 63 (6) (2014) 974–983.
[30] C.R. Ferrone, et al., Radiological and surgical implications of neoadjuvant treatment with FOLFIRINOX for locally advanced and borderline resectable pancreatic cancer, Ann. Surg. 261 (1) (2015) 12–17.
[31] M. Blazer, et al., Neoadjuvant modified (m) FOLFIRINOX for locally advanced unresectable (LAPC) and borderline resectable (BRPC) adenocarcinoma of the pancreas, Ann. Surg. Oncol. 22 (4) (2015) 1153–1159.
[32] C.L. Roland, et al., Neoadjuvant therapy is associated with a reduced lymph node ratio in patients with potentially resectable pancreatic cancer, Ann. Surg. Oncol. 22 (4) (2015) 1168–1175.